Dynamic electrical measurement of biomolecule behavior via plasmonically-excited nanogap fabricated by electromigration

Morita, Akihiro
Sumitomo, Takayuki
Uesugi, Akio
Sugano, Koji
Isono, Yoshitada

(Citation)
Nano Express,2(1):010032

(Issue Date)
2021-03-08

(Resource Type)
journal article

(Version)
Version of Record

Nano Express

Dynamic electrical measurement of biomolecule behavior via plasmonically-excited nanogap fabricated by electromigration

IOP Publishing Nano Express 2 (2021) 010032 https://doi.org/10.1088/2632-959X/abe9c0

NANO EXPRESS

PAPER

Dynamic electrical measurement of biomolecule behavior via plasmonically-excited nanogap fabricated by electromigration

Akihiro Morita, Takayuki Sumitomo, Akio Uesugi, Koji Sugano and Yoshitada Isono

Department of Mechanical Engineering, Graduate School of Engineering, Kobe University, 1-1 Rokkodai-cho, Nada-ku, Kobe 657-8501 Japan

E-mail: sugano@mech.kobe-u.ac.jp

Keywords: plasmonic resonance, plasmonic trapping, DNA, single molecule, nanogap

OPEN ACCESS

RECEIVED
12 December 2020

REVISED
14 February 2021

ACCEPTED FOR PUBLICATION
25 February 2021

PUBLISHED
8 March 2021

Abstract

The dynamic motion of DNA oligomers at the nanoscale gap between nanoelectrodes is measured under plasmonic excitation using laser irradiation. The use of a nanogap enables highly sensitive detection of individual molecules using an electrical readout or an optical readout such as Raman spectroscopy. However, the target molecule must reach the nanogap in order to be detected. This study focuses on the use of plasmonic excitation to trap molecules at the nanogap surface. The nanogap electrode is fabricated by electromigration and is, therefore, a much smaller nanogap than the top-down fabrication in the conventional plasmonic trapping studies. To demonstrate the individual molecule detection and to investigate the molecular behavior, the molecules are monitored using an electrical readout under a bias voltage instead of an optical readout used in the conventional studies. The conductance change due to DNA oligomer penetration to the nanogap is observed with the irradiated light intensity of over 1.23 mW. The single-molecule detection is confirmed irradiating the laser to the nanogap. The results suggest that DNA oligomers are spontaneously attracted and concentrated to the nanogap corresponding to the detection point, resulting in high detection probability and sensitivity.

1. Introduction

A biochemical sensor using a nanogap is a highly sensitive technique by which molecules can be detected at the individual level. An electrical method using a nanogap electrode defined as a pair of nanoelectrodes with a nanometer gap in between them detects biochemical molecules by measuring an electrical conductance change [1–4]. DNA oligomers are a type of molecule that can be measured using a nanogap electrode for DNA sequencing. This technique is expected for the identification of individual nucleotides, as each nucleotide will produce an electrical conductance in a specific conductance range. To achieve single-molecule detection at the nucleotide level, an electrode gap of counter nanoelectrodes should be comparable to the molecular size, which is around 1 nm or less. We also refer a plasmonic method using a nanogap. Surface-enhanced Raman spectroscopy (SERS) is a promising technique for highly sensitive biochemical sensing [5–10]. The method enables single-molecule identification because the Raman spectrum represents a molecular structure. A gold (Au) nanogap is essential for obtaining high sensitivity when performing SERS, as it enhances Raman scattering light from a target molecule due to localization and enhancement of an electromagnetic field at the nanogap by localized plasmonic resonance. The enhancement factor of Raman scattering light is inversely proportional to the nanogap [11]. A reduction in the gap width to 1 nm or less is significantly useful to achieve the sensitivity required for single-molecule identification. Nanoparticle ensembles have frequently been used to form a nanogap of 1 nm or less between particles. It is extremely difficult to fabricate such a small gap by the electron beam (EB) lithography-based top-down process or the focused ion beam (FIB) process [12–16]. These electrical and plasmonic techniques enable us to perform highly sensitive and direct measurements without complicated, costly, and time-consuming preprocessing such as fluorescent labeling.

Although it is often challenging for molecules to reach a small nanogap when the molecules are found in low concentrations, it is possible for nanogaps to detect a single molecule such as DNA oligomers. In most cases of SERS studies using a substrate, measurements are carried out in dry conditions [17, 18]. Target molecules are concentrated at nanogaps after drying solutions. Solution-based single-molecule detection presents a challenge of capturing a target molecule at a nanogap working as a sensing spot. Manipulation and trapping of molecules to a nanogap is an effective way to improve the probability that a molecule reaches a nanogap. Optical trapping by laser focusing restricts the minimum molecular size to be manipulated, resulting in the manipulation of micron size objects such as a cell [19–21]. Plasmonic trapping of molecules has the potential to allow manipulation of nanometer-scale molecules, such as proteins and DNA [22, 23]. This is because the Au plasmonic structure can localize incident light at the nanogap, resulting in much larger optical force due to an enormous electromagnetic field, as mentioned above. This method can detect a single molecule with plasmonic nanogap structures with a nanoaperture or a mechanically-controllable break junction as well as trapping [22–24]. Dielectrophoretic and thermophoretic forces due to the gradient of electromagnetic field from the nanogap have been discussed as a trapping principle [25–30]. The strong dielectrophoretic force is able to be realized by the large gradient of the electromagnetic field that is generated at the nanogap.

The reported plasmonic nanogaps are around 10 nm or more because they are produced by the EB-lithography-based processes or the FIB processes which have a limitation of processing resolution [12–16]. Such a nanogap is insufficiently small in order to realize the detection of individual molecules; the nanogap of around 1 nm or less is required. In addition, to obtain the larger attraction force, the larger electromagnetic enhancement and gradient are required, which is also realized by reduction in nanogap.

In this study, in order to achieve detection of biomolecules such as DNA oligomers at the individual molecular level using the nanogap, we investigated the molecule behavior under light excitation of the nanogap. We focused on a smaller nanogap and an electrical readout in order to trap and detect the individual DNA oligomer. The nanogap was fabricated by electromigration in order for 1 nm or less nanogap [31–34]. It is expected that a smaller nanogap forms a higher electromagnetic enhancement and gradient at the nanogap resulting in the larger plasmonic trapping force of smaller biomolecules with lower light intensity. The effect of light irradiation on the behavior of single DNA oligomers at the nanogap was investigated using an electrical readout instead of the optical readout. We performed the time-series measurement of an electrical current between counter nanoelectrodes.

2. Experimental

2.1. Fabrication

The fabrication process for the gold nanoelectrodes starts from a bare silicon wafer with a thickness of 625 μm. The wafer was thermally oxidized so that the thickness of the silicon dioxide film was 0.8 μm. EB lithography was then performed on the SiO_2 film and then a gold film of 50 nm thickness was deposited via the EB evaporation process. We fabricated the gold nanowire using the lift-off process. The SEM image is shown in figure 1(a). The nanowire was then broken by electromigration. The applied voltage was gradually increased until the current abruptly dropped off. The SEM images of the fabricated nanoelectrodes are shown in figures 1(b) and (c).

2.2. Characterization

We characterized the fabricated nanoelectrode after breaking by electromigration. The current-voltage (I–V) characteristic was measured as shown in figure 1(d). The interspace distance at the nanogap was estimated by fitting the experimental results to the Fowler–Nordheim equation based on the tunneling current. We observed the exponential increase in current up to the bias voltage of 4.4 V.

The Fowler–Nordheim equation is represented as follows [35, 36].

$$I = \frac{Ae^3E^2}{8\pi\hbar\phi t^2(y)} \exp\left[-\frac{8\pi\sqrt{2m}\,\phi^{\frac{3}{2}}}{3e\hbar E}\nu(y)\right] \tag{1}$$

Here, A is the counter area of the nanogap, e is the electron charge, $\hbar$ is the reduced Planck constant, ϕ is a work function of gold, m is the mass of electron. $E = \beta V/d$ is an electric field with the field enhancement factor β, where V and d are the bias voltage and the nanogap, respectively [37–40]. $t(y) = 1 + 0.1107y^{1.33}$ and $\nu(y) = 1 - y^{1.69}$ are compensation terms considering the mirror images of the electrode surfaces. Here, y is represented as $y = (1/\phi)\sqrt{(e^3E/4\pi\varepsilon_0)}$, where ε_0 is the permittivity of vacuum. The nanogap d was used as a parameter for the fitting curve. In this study, we assume that the electrode tip at the nanogap is a semispherical shape. Some papers have reported that the enhancement factor is represented by the aspect ratio [38–40]. In this study, the enhancement factor is regarded as the aspect ratio of 1 and $\beta = 1$. The experimental I-V characteristic was consistent with the fitting curve. From the exponential increase and good agreement, we consider that the

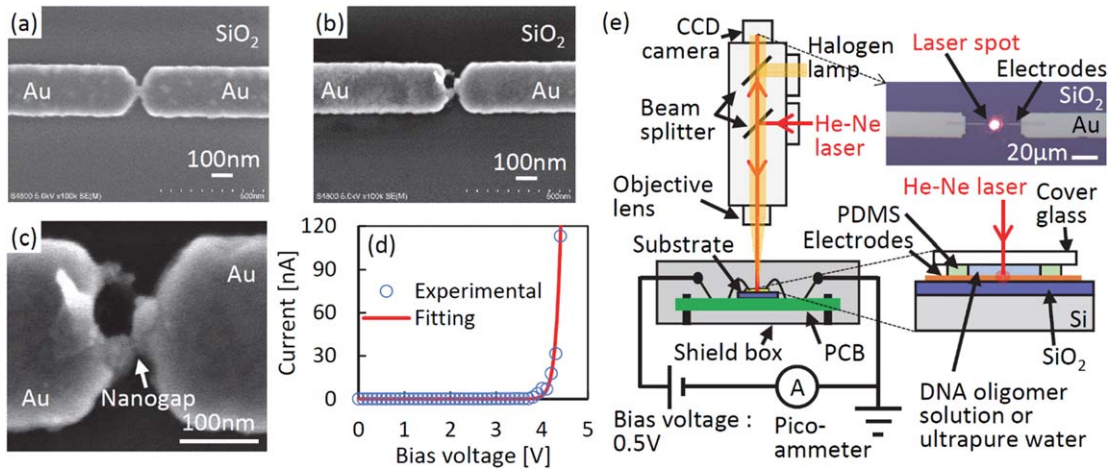

Figure 1. Fabrication and electrical characterization of the fabricated nanoelectrode. (a)–(c) SEM images of gold nanoelectrode (a) before and (b), (c) after electromigration, fabricated on the SiO_2 thin film. Scale bars indicate 100 nm. (d) Experimental Current-voltage (I–V) curve and calculated fitting curve using Fowler–Nordheim equation for tunneling current evaluation. (e) Schematic diagram of the experimental set-up to acquire time-series data of current. He-Ne laser was used for excitation of nanogap. The current was measured by a picoammeter under the bias voltage of 0.5 V. The fabricated nanoelectrodes were wire-bonded to the printed-circuit board and then placed inside the shield box. Solution reservoir for ultrapure water and DNA solution was fabricated on the substrate using the PDMS frame and the cover glass. The microscope image of the electrodes and the laser spot was also shown. Scale bar indicates 20 μm.

nanogap and the wiring structures held without melting and breaking against the current at the bias voltage up to 4.4 V. We obtained the gap d of 0.37 nm from the fitting result. We confirmed the nanogap that possessed tunneling current characteristics.

2.3. Measurements

We measured the time-series data of the electrical current (I-t) when applying the bias voltage. The polydimethylsiloxane (PDMS) frame was applied to the substrate as shown in figure 1(e). The DNA oligomer solution or ultrapure water was injected into the PDMS frame, and the cover glass was then placed onto the frame. The DNA oligomer concentration and sequence were 10 μM and 5′-AAAAAAAAAAAAAAA-3′ (Fasmac Co., Ltd), respectively.

We used the He-Ne laser of 632.8 nm wavelength to excite the nanogap. It is because the plasmonic excitation at a nanogap by 632.8 nm laser was confirmed by the SERS experiments using a nanoparticulate system [5–7]. The nanogap was located at the laser spot and the focus point. The laser intensity was set to 0, 0.74×10^{-3}, 0.11, 1.23, 4.36, 7.05, and 11.4 mW. The diameter of the laser spot was approximately 8.8 μm. The calculated power density of the laser was 18.9 kW cm^{-2} at the laser intensity of 1.23 mW. The SERS studies on DNA oligomers detection used 6–12 mW laser irradiation [41, 42]. Therefore, the laser irradiation used in this study is thought to give no damage to DNA oligomers.

The bias voltage and the sampling rate were set to 0.5 V [1–3] and 1 kHz, respectively. We carried out 9 measurements for each laser intensity. The duration time of measurement was 60 s for each measurement.

3. Results and discussions

3.1. Time-series current measurements

We obtained time-series data of measured current from ultrapure water and DNA solution varying a laser intensity, as shown in figure 2, with the measured current ranging from approximately 0 to 4 nA. A constant current was observed in both the cases of ultrapure water and DNA solution under no laser irradiation, as shown in figure 2(a), indicating that no molecule enters the nanogap. We obtained the electrical signal from the DNA solution at the laser intensity of over 1.23 mW, as shown in figures 2(b)–(d), although the ultrapure water exhibited the constant current despite the use of laser irradiation. The current transition indicates that a DNA oligomer has entered the nanogap.

We identified two kinds of typical patterns of the current transition. The first was a step-like pattern, as shown in figures 2(b) and (c). Upon measuring the discrete levels of current, we generated histograms of current acquired from DNA solution as shown on the left side of each graph in figure 2. The current interval in the histogram was set to 0.001 nA. Notably, there were some distinguishable peaks observed in the histogram as shown in figures 2(b) and (c). According to these results, we confirmed that the fabricated nanogap displays

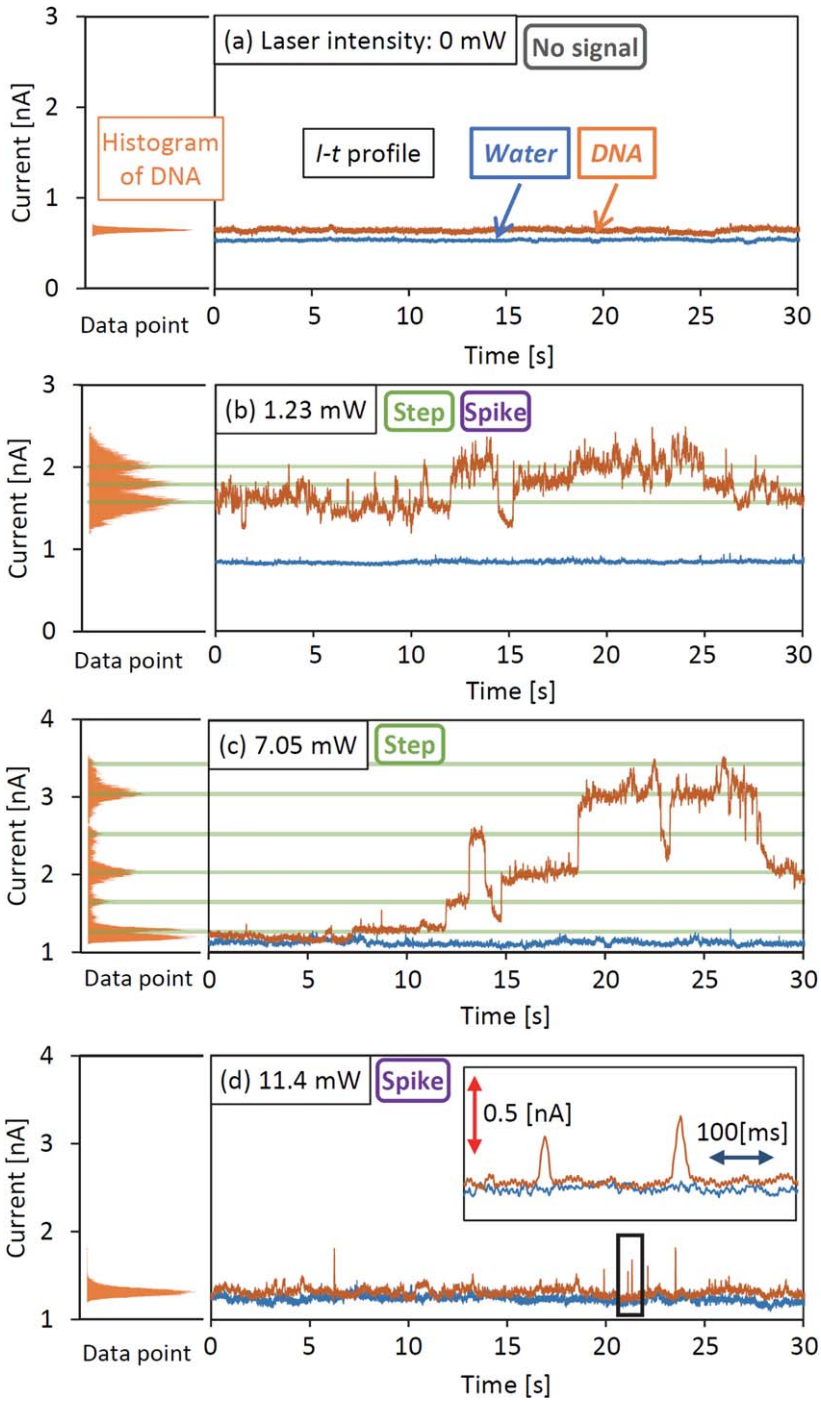

Figure 2. Time-series data of measured electrical current (I-t profile) from ultrapure water (blue line) and DNA solution (orange line) at laser intensity of (a) 0 mW, (b) 1.23 mW, (c) 7.05 mW, and (d) 11.4 mW. The histograms of the acquired current data from DNA solution (orange) also are shown on the left side of the time-series data. Graph (b) and (c) show the step-like pattern in the time-series current data and more than two peaks in the histgrams, indicating a step-by-step detection.

single-molecule sensitivity of DNA oligomers and it was realized by the laser irradiation of 1.23 mW or more. An increase of more than two steps from the lowest current peak level, namely more than two peaks, in the time-series data of currents indicates the step-by-step collection of more than two DNA oligomers at the nanogap. The duration of the constant current suggests that DNA oligomers had stagnated at the nanogap for a long period of time. The second pattern that we observed was a spike-like pattern, as shown in figures 2(b) to (d). Figure 2(d) also shows the magnified graph for the spike-like signals in the inset. These findings suggest that the DNA oligomers passed through a nanogap without stagnation.

Figure 3(A) shows the average of current with ultrapure water as a function of laser intensity, indicated by the blue lines in figure 2. The current with ultrapure water, shown as a baseline of time-series data of measured current in figure 2, increased with laser intensity. This is because the temperature of the solution at the nanogap

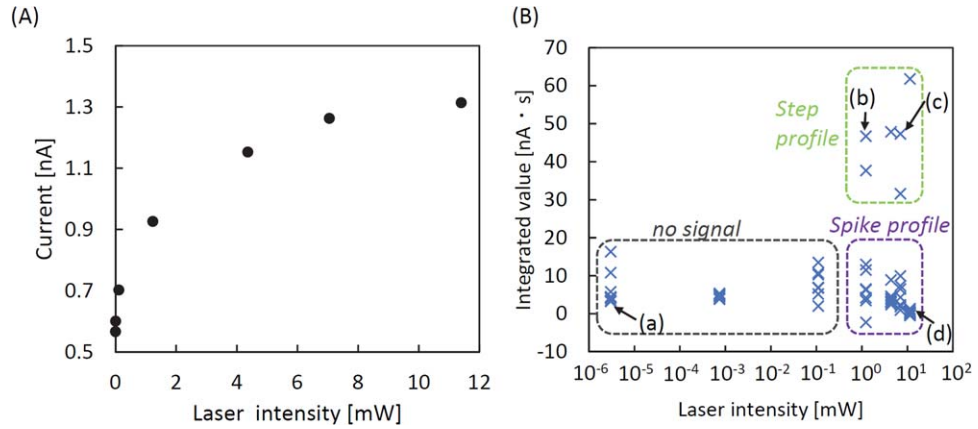

Figure 3. Background and DNA measurement current. (A) Background average current at a sampling rate of 1 kHz in 60 s with ultrapure water as a function of laser intensity. (B) Individual integrated values of time-series current data depending on laser intensity. The ultrapure water data was subtracted as the background value from the DNA oligomer solution data. Point (a) indicates the no-signal data without laser irradiation. The data are plotted at the laser intensity of 3 nW, which is the indicated value of the intensity sensor. Points (b) and (c) indicate the step-profile data. Point (d) indicates the spike-profile data.

was increased with laser intensity due to the light absorption effect by photothermal conversion of light irradiation, resulting in increased conductivity [28]. The time-series data of the current was integrated at 60 s for the DNA oligomer solution. The ultrapure water data was then subtracted from the DNA oligomer solution data as the background value. The calculation results as a function of laser intensity are shown in figure 3(A). Data points of (a) to (d) in figure 3(B) correspond to the graphs (a) to (d) in figure 2, respectively. In the region including (a) in figure 3(B), we confirmed that the integrated value is small, indicating that no DNA fragment could enter the nanogap. We observed two separate regions of integrated values at a laser intensity of more than 1.23 mW. In the region including (b) and (c) at a laser intensity of more than 1.23 mW, an increase in the current level was observed, indicating laser irradiation concentrates molecules to a nanogap. The region including (d), which shows smaller integrated value even at values higher than 1.23 mW, corresponds to the spike-like signals. However, certain data points of the integrated values remained low even at these higher values. The effect of the heat generated by the laser light is greater than the plasmonic optical force. We assume that the Brownian motion enhanced due to the increase in temperature during laser irradiation, and stagnation times are shorter in the nanogap.

The effect of high-power laser irradiation on the nanogap structure is discussed in this paragraph. After the 11.4 mW laser irradiation, we confirmed the same current levels during the repetitive measurement at the laser intensity from 0 to 11.4 mW. The dependency of the current level of the ultrapure water on the laser intensity as shown in figure 2(a) exhibited no change after 11.4 mW laser irradiation. From these results, the nanogap structure change due to the laser irradiation was thought to be negligible.

3.2. Event frequency

Next, we reported the event frequency at which the DNA oligomers enter or exit from the nanogap. The position and the angle at which the DNA oligomers enter the nanogap is not constant. For this reason, the current transition of transporting in the nanogap has a variation. We defined the change of current ΔI as $\Delta I = |I(t) - I(t - \Delta t)|$. We defined that a DNA oligomer enters and exits the nanogap when $\Delta I \geqslant A_t$, with A_t representing the threshold current. Here, we focused on the histogram shown on the left side of the graph in figure 2. Figure 4(a) shows an example of a current histogram, and observed discrete peak currents. We acquired the interval of the current change depending on the laser intensity as shown in figure 4(b). The red dotted line in figure 4(b) indicates a linear fitting line by least squares method. The threshold current A_t was defined by the fitting line. When the current change in a measured signal exceeds the threshold current, we determined that a DNA oligomer enters or exits from the nanogap. We calculated the number of events at each laser intensity. Similar to the integration results shown in figure 3(B), we confirmed that many data points exceeded the threshold when the laser intensity was 1.23 mW or more, as shown in figure 5.

The trapping and detection frequency is thought to increase with a concentration of DNA oligomers. The attraction force is a short-range action so that molecules close to the nanogap are attracted. The trapping and the detection are stochastic events. Therefore, the event frequency has some variation as shown in figures 3(b) and 5. The variation is thought to depend on a concentration of DNA oligomers.

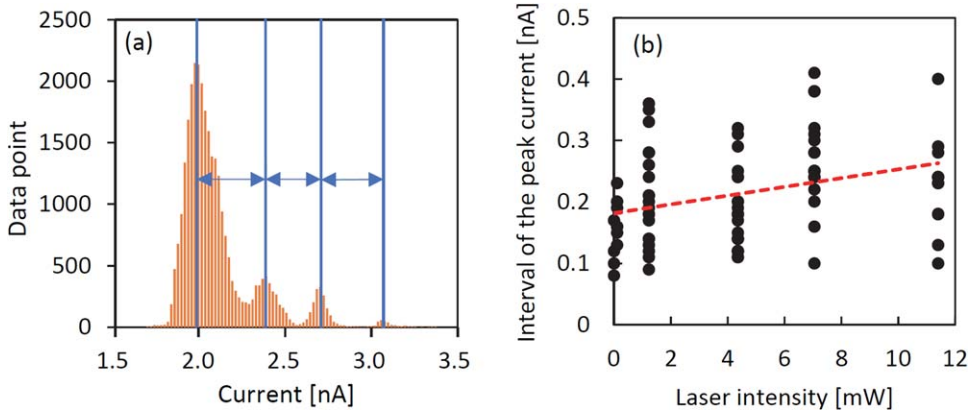

Figure 4. Histogram showing the current in 30 s measurement at 1.23 mW laser irradiation (a) and interval of the peak current as a function of laser intensity (b). Red dotted line indicates linear fitting result in (b).

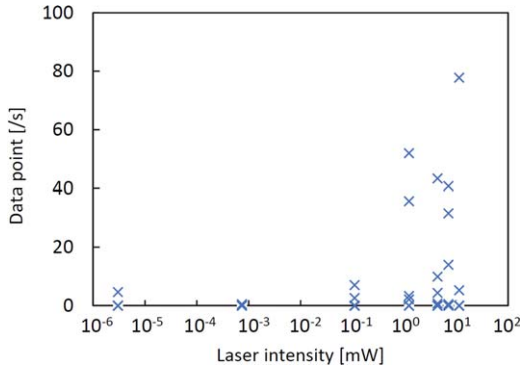

Figure 5. Frequency of data points exceeding the threshold level of current as a function of laser intensity.

From the experimental result, we demonstrate that DNA oligomers were attracted to the nanogap by laser light irradiation. It can be suggested that the dielectrophoretic force generated by laser light irradiation promotes the travel of DNA oligomers in the direction of the nanogap. This phenomenon is significantly useful for sensing applications. The results suggest that DNA oligomers are spontaneously attracted and concentrated to the nanogap corresponding to the detection point, resulting in high detection probability and sensitivity.

3.3. Stagnation time

In this study, we also measured stagnation time via histogram analysis. The interval time between molecule penetration and exit is defined as the stagnation time, as shown in figure 6(a). The histograms shown in figure 6 have different range settings an interval of the stagnation time. We found the peak at about 22 ms of the stagnation time in figure 6(c). This suggests that the spike-like signals distribute from 0 to around 40 ms, and exhibit peak stagnation time at 22 ms. We considered the short stagnation time to detect DNA oligomers when transporting through the nanogap. According to the histogram shown in figure 6(d), the number of data points in the histogram decreased with increasing stagnation time.

Next, we discuss the stagnation time as a function of laser intensity. Figure 7 shows the histograms of the stagnation time ranging from 0 to 50 ms focusing on the short-time stagnation. The solid lines indicate the normal distribution calculated extracting the stagnation time of 0–40 ms for discussion of spike-like signals. The peak stagnation times were found at 22.5, 21.5, 22.1, and 21.2 ms at the laser intensity of 0.11, 1.23, 4.36, 7.05 mW, and 11.4 mW, respectively. The average stagnation time shows no difference at the laser intensity of 0.11or more.

Figure 8 shows the number of events as a function of laser intensity. The range of the stagnation time varies in figure 8. The number of events for each intensity exhibits the same tendency shown in figure 5. At the laser intensity of 1.23 mW or more, the number of events has no large difference.

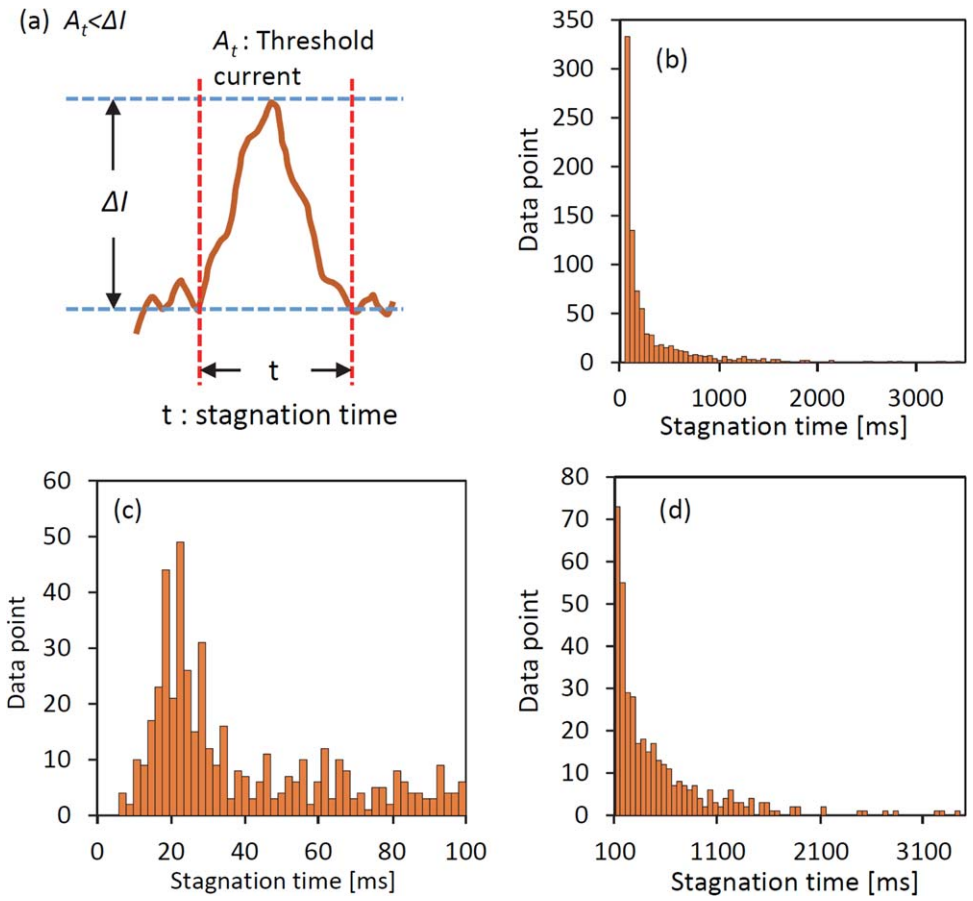

Figure 6. Stagnation time distribution. (a) Definition of current change and stagnation time. (b)–(d) Histograms of stagnation time with stagnation time ranging from 0 to 3500 ms with an interval of 50 ms (b), from 0 to 100 ms with an interval of 2 ms (c), and from 100 to 3500 ms with an interval of 50 ms (d).

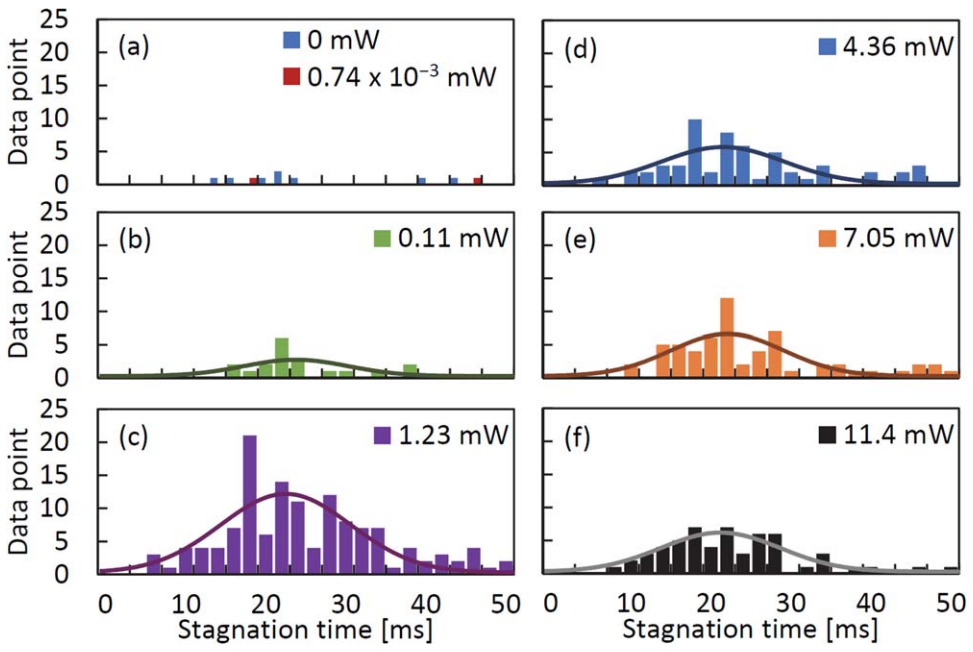

Figure 7. Histograms of stagnation time ranging from 0 to 50 ms focusing on the short-time stagnation depending on the laser intensity. The laser intensity are (a) 0 and 0.74 $\times$ 10^{-3}, (b) 0.11, (c) 1.23, (d) 4.36, (e) 7.05, and (f) 11.4 mW. The solid lines indicate the normal distribution calculated extracting the stagnation time of 0–40 ms for discussion of spike-like signals.

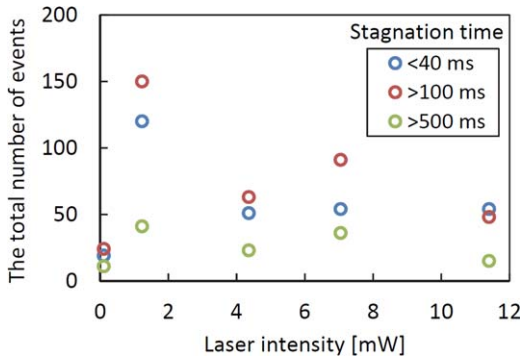

Figure 8. The number of events as a function of laser intensity ranging from 0.11 to 11.4 mW. The range of the stagnation time was varied for less than 40 ms, more than 100 ms, and more than 500 ms.

Notably, adenine molecules adsorb to the gold surface, and we hypothesized that DNA oligomers switch between adsorption and desorption on a gold surface at the nanogap [43]. Moreover, it has been suggested that the adsorption time on the nanogap surface can determine the stagnation time.

4. Conclusion

In this study, we investigated the effect of nanogap laser irradiation on DNA oligomer behavior using the electrical readout instead of the optical readout used in the conventional studies. We fabricated the gold nanoelectrode with the nanogap using an EB-lithography-based, lift-off technique and subsequent electromigration. The fabricated nanoelectrode was evaluated from the measured I-V curve. By fitting the experimental results by the Fowler–Nordheim equation, we confirmed that the nanogap is small enough to achieve the tunneling current property. The time-series data of the current was measured under the applied bias voltage of 0.5 V. We observed that the current increased by more than 1.23 mW laser intensity when the DNA solution was placed on the substrate. From these results, we confirmed that laser irradiation to the nanogap enables to attract the molecules to the nanogap, and to detect the DNA oligomer with single-molecule sensitivity. This ability can be attributed to the dielectrophoresis force generated from plasmonic excitation of the nanogap. The histogram generated from the time-series experiment measuring the current revealed that the stagnation time peaked at 22 ms. Moreover, the plasmonically-excited nanogap is an extremely useful tool to concentrate and detect individual biochemical molecules, such as a DNA oligomer.

Acknowledgments

A part of this study was supported by Micro/Nano Fabrication Hub in Kyoto University funded by the Ministry of Education, Culture, Sports, Science and Technology (MEXT), Japan. A part of this study was supported by JSPS KAKENHI Grant Number JP18H01847 and 19H02571.

Data availability statement

The data that support the findings of this study are available upon reasonable request from the authors.

ORCID iDs

Akio Uesugi https://orcid.org/0000-0002-7913-3679
Koji Sugano https://orcid.org/0000-0002-0780-0110
Yoshitada Isono https://orcid.org/0000-0003-2370-3246

References

[1] Tsutsui M, Taniguchi M, Yokota K and Kawai T 2010 Identifying single nucleotides by tunnelling current *Nat. Nanotechnol.* **5** 286
[2] Tsutsui M, He Y, Furuhashi M, Rahong S, Taniguchi M and Kawai T 2012 Transverse electric field dragging of DNA in a nanochannel *Sci. Rep.* **2** 394

[3] Ohshiro T, Matsubara K, Tsutsui M, Furuhashi M, Taniguchi M and Kawai T 2012 Single-molecule electrical random resequencing of DNA and RNA *Sci. Rep.* **2** 501
[4] Ohshiro T, Komoto Y, Konno M, Koseki J, Asai A, Ishii H and Taniguchi M 2019 Direct analysis of incorporation of an anticancer drug into DNA at single-molecule resolution *Sci Rep.* **9** 3886
[5] Sugano K, Suekuni K, Takeshita T, Aiba K and Isono Y 2015 Surface-enhanced Raman spectroscopy using linearly arranged gold nanoparticles embedded in nanochannels *Jpn. J. Appl. Phys.* **54** 06FL3
[6] Sugano K, Aiba K, Ikegami K and Isono Y 2017 Single-molecule surface-enhanced Raman spectroscopy of 4,4′-bipyridine on a prefabricated substrate with directionally arrayed gold nanoparticle dimers *Jpn. J. Appl. Phys.* **56** 06GK1
[7] Sugano K, Ikegami K and Isono Y 2017 Characterization method for relative Raman enhancement for surface-enhanced Raman spectroscopy using gold nanoparticle dimer array *Jpn. J. Appl. Phys.* **56** 06GK3
[8] Kneipp J, Kneipp H and Kneipp K 2008 SERS—a single-molecule and nanoscale tool for bioanalytics *Chem. Soc. Rev.* **37** 1052–60
[9] Pieczonka N P and Aroca R F 2008 Single molecule analysis by surfaced-enhanced Raman scattering *Chem. Soc. Rev.* **37** 946–54
[10] Qian X M and Nie S M 2008 Single-molecule and single-nanoparticle SERS: from fundamental mechanisms to biomedical applications *Chem. Soc. Rev.* **37** 912–20
[11] Tong L, Xu H and Käll M 2014 Nanogaps for SERS applications *MRS Bull.* **39** 163–8
[12] Al Balushi A A and Gordon R 2014 Label-free free-solution single-molecule protein–small molecule interaction observed by double-nanohole plasmonic trapping *ACS Photonics* **1** 389–93
[13] Pang Y and Gordon R 2012 Optical trapping of a single protein *Nano Lett.* **12** 402–6
[14] Yoo D, Gurunatha K L, Choi H K, Mohr D A, Ertsgaard C T, Gordon R and Oh S H 2018 Low-power optical trapping of nanoparticles and proteins with resonant coaxial nanoaperture using 10 nm gap *Nano Lett.* **18** 3637–42
[15] Jones S, Andrén D, Karpinski P and Käll M 2018 Photothermal heating of plasmonic nanoantennas: influence on trapped particle dynamics and colloid distribution *ACS Photonics* **5** 2878–87
[16] Zhang C, Li J, Belianinov A, Ma Z, Kyle Renshaw C and Gelfand R M 2018 Nanoaperture fabrication in ultra-smooth single-grain gold films with helium ion beam lithography *Nanotechnology* **31** 465302
[17] Nie S and Emory S R 1997 Probing single molecules and single nanoparticles by surface-enhanced Raman scattering *Science* **275** 1102–6
[18] Imura K, Okamoto H, Hossain M K and Kitajima M 2006 Visualization of localized intense optical fields in single gold-nanoparticle assemblies and ultrasensitive Raman active sites *Nano Lett.* **6** 2173–6
[19] Wang M, Zhao C, Miao X, Zhao Y, Rufo J, Liu Y J, Huang T J and Zheng Y 2015 Plasmofluidics: merging light and fluids at the micro-/nanoscale *Small* **11** 4423–44
[20] Ghosh S and Ghosh A 2020 Next-generation optical nanotweezers for dynamic manipulation: from surface to bulk *Langmuir* **36** 5691–708
[21] Bradac C 2018 Nanoscale optical trapping: a review *Adv. Opt. Mater.* **6** 1800005
[22] Kotnala A and Gordon R 2014 Quantification of high-efficiency trapping of nanoparticles in a double nanohole optical tweezer *Nano Lett.* **14** 853–6
[23] Gordon R 2019 Biosensing with nanoaperture optical tweezers *Opt. Laser Technol.* **109** 328–35
[24] Zhan C, Wang G, Yi J, Wei J-Y, Li Z-H, Chen Z-B, Shi J, Yang Y, Hong W and Tian Z-Q 2020 Single-molecule plasmonic optical trapping *Matter* **3** 1350–60
[25] Shoji T, Saitoh J, Kitamura N, Nagasawa F, Murakoshi K, Yamauchi H, Ito S, Miyasaka H, Ishihara H and Tsuboi Y 2013 Permanent fixing or reversible trapping and release of DNA micropatterns on a gold nanostructure using continuous-wave or femtosecond-pulsed near-infrared laser light *J. Am. Chem. Soc.* **135** 6643–8
[26] Shoji T and Tsuboi Y 2014 Plasmonic optical tweezers toward molecular manipulation: tailoring plasmonic nanostructure, light source, and resonant trapping *J. Phys. Chem. Lett.* **5** 2957–67
[27] Pin C, Ishida S, Takahashi G, Sudo K, Fukaminato T and Sasaki K 2018 Trapping and deposition of dye-molecule nanoparticles in the nanogap of a plasmonic antenna *ACS Omega* **3** 4878–83
[28] Nicoli F, Verschueren D, Klein M, Dekker C and Jonsson M P 2014 DNA translocations through solid-state plasmonic nanopores *Nano Lett.* **14** 6917–25
[29] Hoshina M, Yokoshi N, Okamoto H and Ishihara H 2017 Super-resolution trapping: a nanoparticle manipulation using nonlinear optical response *ACS Photonics* **5** 318–23
[30] Belkin M, Chao S-H, Jonsson M P, Dekker C and Aksimentiev A 2015 Plasmonic nanopores for trapping, controlling displacement, and sequencing of DNA *ACS Nano* **9** 10598–611
[31] Strachan D R, Smith D E, Johnston D E, Park T H, Therien M J, Bonnell D A and Johnson A T 2005 Controlled fabrication of nanogaps in ambient environment for molecular electronics *Appl. Phys. Lett.* **86** 043109
[32] Hadeed F O and Durkan C 2007 Controlled fabrication of 1–2 nm nanogaps by electromigration in gold and gold-palladium nanowires *Appl. Phys. Lett.* **91** 123120
[33] Johnston D E, Strachan D R and Johnson A C 2007 Parallel fabrication of nanogap electrodes *Nano Lett.* **7** 2774–7
[34] Xiang C, Kim J Y and Penner R M 2009 Reconnectable sub-5 nm nanogaps in ultralong gold nanowires *Nano Lett.* **9** 2133–8
[35] Hishinuma Y, Geballe T H, Moyzhes B Y and Kenny T W 2001 Refrigeration by combined tunneling and thermionic emission in vacuum: use of nanometer scale design *Appl. Phys. Lett.* **78** 2572–4
[36] Banerjee A, Hirai Y, Tsuchiya T and Tabata O 2017 Measurement and potential barrier evolution analysis of cold field emission in fracture fabricated Si nanogap *Jpn. J. Appl. Phys.* **56** 06GF
[37] Kokkorakis G C, Modinos A and Xanthakis J P 2002 Local electric field at the emitting surface of a carbon nanotube *J. Appl. Phys.* **91** 4580–4
[38] Wang M, Li Z H, Shang X F, Wang X Q and Xu Y B 2005 Field-enhancement factor for carbon nanotube array *J. Appl. Phys.* **98** 014315
[39] Bocharov G S and Eletskii A V 2013 Theory of carbon nanotube (CNT)-based electron field emitters *Nanomaterials* **3** 393–442
[40] Forbes R G 2017 The theoretical link between voltage loss, reduction in field enhancement factor, and Fowler-Nordheim-plot saturation *Appl. Phys. Lett.* **110** 133109
[41] Huang J A, Mousavi M Z, Zhao Y, Hubarevich A, Omeis F, Giovannini G, Schutte M, Garoli D and De Angelis F 2019 *Nat. Commun.* **10** 5321
[42] Chen C, Li Y, Kerman S, Neutens P, Willems K, Cornelissen S, Lagae L, Stakenborg T, Van and Dorpe P 2018 *Nat. Commun.* **9** 1733
[43] Liu J 2012 Adsorption of DNA onto gold nanoparticles and graphene oxide: surface science and applications *Phys. Chem. Chem. Phys.* **14** 10485–96